Applied Clay Science 255 (2024) 107422

Contents lists available at ScienceDirect

Applied Clay Science

journal homepage: www.elsevier.com/locate/clay

Technical note

Technological study of kaolinitic clays from Fms. Escucha and Utrillas to be used in dermo-pharmaceutical products

Ismael Monterde Cortés [a], Raquel de Melo Barbosa [b,*], Fátima García-Villén [a], Ignacio Moya Ramírez [c], Marina Massaro [d], Serena Riela [e], Alberto López-Galindo [f], César Viseras [a,f], Rita Sánchez-Espejo [a]

[a] Department of Pharmacy and Pharmaceutical Technology, School of Pharmacy, Campus of Cartuja s/n, University of Granada, 18071 Granada, Spain
[b] Department of Pharmacy and Pharmaceutical Technology, School of Pharmacy, C/Profesor García González, 2. 41012 Seville, Spain
[c] Departmento de Ingeniería Química, Universidad de Granada, 18071 Avda. Fuentenueva s/n, Granada, Spain
[d] Dipartimentodi Scienze e Tecnologie Biologiche, Chimiche e Farmaceutiche (STEBICEF) University of Palermo, V. le delle Scienze, Ed. 17 "StanislaoCannizzaro", 90128 Palermo, Italy
[e] Dipartimentodi Scienze Chimiche University of Catania, Via A. Doria, 6, 95125 Catania, Italy
[f] Andalusian Institute of Earth Sciences, CSIC-University of Granada, Av. de Las Palmeras, Armilla, 18100 Granada, Spain

ARTICLE INFO

Keywords:
Kaolinitic clay
Clay properties
Dispersed systems
Health applications
Fms. Escucha and Utrillas

ABSTRACT

The present study aims to evaluate five clay samples from different pits in the Teruel province, Spain. While these clays are primarily utilized as raw materials in ceramics, their potential applications in pharmaceutical and cosmetic domains, notably in sun protection and thermal mud products, are under investigation. Characterization of these clays entailed X-ray diffraction, X-ray fluorescence, scanning electron microscopy, pH measurement, analysis of technological properties, rheological assessment, and thermal property evaluation. Furthermore, given the predominant composition of kaolin in most of the samples, their Sun Protection Factor (SPF) in suspensions and physical stability were assessed. The studied samples exhibited varied mineralogical compositions, primarily consisting of kaolinite (70% to 15%), quartz (75% to 5%), and illite (26% to 7%). The pH values of these dispersions closely matched the skin's pH, exhibiting anti-thixotropic behavior at 50% *w*/w and demonstrating suitable viscosity for skin application. Based on their composition and rheological properties, the samples exhibited potential for use as therapeutic thermal muds. Analyses of cooling kinetics were performed to validate this potential. Results showed that the dispersions systems attained temperatures between 33.89 °C and 34.62 °C within 20 min (the common application time for thermal muds) and reached 32 °C (skin temperature) in 24.3 to 26.22 min, confirming their appropriateness as therapeutic muds. The SPF values of the dispersions varied from 7.46 to 16.65, with the majority of samples showing significant stability during 45 h. Consequently, it can be inferred that most of the studied samples show advantageous characteristics for inclusion in topical formulations, especially in sun protection and thermal mud products.

1. Introduction

Clays have been used since prehistory, from Mesopotamia and Egyptian times to the present day, to treat various human conditions, including skin, traumatological, and gastrointestinal conditions (Carretero et al., 2006a, 2006b; Perea, 2014; Gomes, 2017; Carretero, 2020). Among the different types of clays used in the pharmaceutical and cosmetic fields, kaolinite possesses physical, chemical, mechanical, and structural properties that make it suitable for various industrial and pharmaceutical applications.

Kaolinite is characterized by its simple structure, special technological, physical, and chemical properties. Chemically, it is a hydrated aluminum silicate with a structural formula of $Al_2Si_2O_5(OH)_4$, belonging to the group of 1:1 phyllosilicate, which consist of a tetrahedral layer and an octahedral layer (TO type) (Brigatti et al., 2013), which are fundamental for its chemical stability and application versatility. The

* Corresponding author.
E-mail addresses: ismaelmonterde@correo.ugr.es (I.M. Cortés), rdemelo@us.es (R. de Melo Barbosa), fgarvillen@ugr.es (F. García-Villén), ignaciomr@ugr.es (I.M. Ramírez), marina.massaro@unipa.it (M. Massaro), serena.riela@unict.it (S. Riela), alberto.lopez@csic.es (A. López-Galindo), cviseras@ugr.es (C. Viseras), ritamsanchez@ugr.es (R. Sánchez-Espejo).

https://doi.org/10.1016/j.clay.2024.107422
Received 14 February 2024; Received in revised form 12 May 2024; Accepted 15 May 2024
Available online 17 May 2024

unique physical properties of kaolinite, such as its particle size and specific surface area, enhance its functionality in formulations requiring intense interaction with other components (Murray, 2000). Furthermore, the mechanical properties of kaolinite, including its compressive and tensile strength augment its applications, providing a reliable and stable material in contexts that necessitate structural robustness and precise chemical and physical interactions. These attributes make kaolinite particularly suited for pharmaceutical and cosmetic applications, where efficacy and safety are paramount (Carretero and Pozo, 2010; López-Galindo et al., 2011; Awad et al., 2017a).

For this study, various samples of kaolinitic clay supplied by EUROARCE® company were used. The term "kaolinitic clay" refers to sedimentary clays composed of a significant amount of kaolinite along with other associated detrital minerals such as micas, feldspars, and iron oxides (Bartolomé, 1997). These Teruel kaolinitic clays are found in the Fms. Escucha and Utrillas (Spain) and are associated with exploitable coal levels. They are currently exploited and used as raw materials in the ceramic sector (Aguilar et al., 1971; Querol, 1990).

In order to use clays for pharmaceutical or cosmetic purposes, they have to meet a series of requirements specified in the main pharmacopoeias (British, European, American, or Japanese). These requirements include tests or trials based on the study of mineralogy and chemical composition, colour, organic impurities, adsorption power, zeta potential, swelling power, or loss on ignition. Additionally, other properties such as particle size distribution, rheological properties, humidity, or specific heat values need to be considered (López-Galindo et al., 2007; Rowe et al., 2009).

Clay minerals, including kaolinite, are used in solid and semi-solid forms in various pharmaceutical and cosmetic preparations. Kaolinite, due to its various properties, is used as an excipient or active ingredient in the pharmaceutical industry (Carretero, 2002; Viseras et al., 2007; López-Galindo et al., 2007; Awad et al., 2017b; Hernández et al., 2019).

The interactions between kaolinite particles and other components in pharmaceutical and/or cosmetic formulations are significantly influenced by particle size, surface charge, and mineral composition (Tang et al., 2016, 2022; Ataytür et al., 2024). Smaller particle sizes of kaolinite increase the surface area available for adsorption, enhancing the mineral's ability to interact with and stabilize other molecules in the formulation. This property is crucial in systems designed for controlled release and emulsion stabilization, where increased surface area directly contributes to improved efficacy and stability of the products (Carretero et al., 2006a, 2006b). Additionally, the surface charge of kaolinite influences electrostatic interactions with active ingredients, which are essential for modifying the release profiles of drugs, as observed in the varied Sun Protection Factor (SPF) results among the samples (López-Galindo et al., 2007). Moreover, the mineral composition of kaolinite, particularly the presence of impurities like quartz and illite, affects not only the mechanical strength and structural integrity of the formulations but also their aesthetic qualities, such as whiteness and texture (Bergaya and Lagaly, 2013). These practical implications emphasize the importance of optimizing kaolinite properties such as particle size distribution and purity to enhance the performance and consumer acceptability of dermo-pharmaceutical products. The diverse SPF values and rheological properties observed across the kaolinitic clay samples further underline the potential for specialized therapeutic applications, reinforcing the need for tailored property adjustments based on the specific end-use (Murray, 2000).

With these premised, the objective of this work is to characterize clay samples from various pits located in the province of Teruel to evaluate their properties for use in the pharmaceutical and cosmetic fields, aiming to provide added value to their current use exclusively focused on the ceramic sector. This study represents the first characterization of Teruel's kaolinitic clays for potential applications in the health field.

2. Geological context

Teruel's mining district is located in Spain, between the southern Aragonesa Branch of the Iberian Mountain Range and the south of the Costero-Catalana Mountain Range, in the so-called "Zona de Enlace" (Guimerá, 1984; Querol et al., 1992). The clays that are the object of study come from the "Escucha" Formation (Upper Aptian-Lower Albian) and "Utrillas" Formation (Lower Albian-Cenomanian), extracted from the pits belonging to EUROARCE® company in the villages of Estercuel, Oliete, and Castellote (Province of Teruel, Aragon, Spain) (Fig. 1). These clays are currently only used in the traditional ceramics industry. The pits are located in the Oliete and Castellote subbasin, which was formed during the Lower Cretaceous in an event of tectonic reactivation in a listric extensional fault system, leading to the subdivision of the main basin, the Maestrazgo Basin, into different subbasins (Aguilar et al., 1971; Cervera et al., 1976; Pardo, 1979).

The Escucha Formation and Utrillas Formation (Fm. Escucha and Fm. Utrillas) were initially defined by Aguilar et al. in 1971 (Aguilar et al., 1971). Later, Cervera et al. (1976) and Pardo et al. (1979) subdivided the Escucha Formation into three Members (Cervera et al., 1976; Pardo, 1979). The Lower Member consists of carbonaceous loams, detrital limestones, coal levels, silts, and sands. The Middle Member is composed of carbonaceous clays together with levels of carbon. The Upper Member is constituted by a clay interval together with silts and sand.

The Fm. Utrillas is located on the top of Fm. Escucha and is characterized by the presence of white and yellowish sands with kaolinitic matrix, together with levels of silts and sands. Traditionally, Querol (1990), Querol et al. (1992) and Pardo et al. (1979) (Pardo, 1979; Querol, 1990; Querol et al., 1992) interpreted the Fm. Escucha as a deltaic-estuarine system, while Pardo (1979)(Pardo, 1979) interpreted the Fm. Utrillas as a fluvial system. However, recent studies have challenged this classic interpretation, and Rodríguez-López et al. (2009) indicated that the upper part of the Fm. Escucha and Fm. Utrillas constitute the sedimentary record of the first sandy desert system of the Cretaceous in Europe (Rodríguez-López et al., 2009).

During the deposition of the Fms. Escucha and Utrillas, the kaolinitic formation occurred under dry climatic conditions in a tropical latitude (Chumakov et al., 1995; Meléndez et al., 2009; Rodríguez-López et al., 2010). The Oliete and Castellote subbasins received an amount of materials rich in feldspar and other minerals, like mica. Due to these climatic conditions, the clays present in these formations have properties suitable for their application in pelotherapy and cosmetics (Bartolomé, 1997; López-Galindo and Viseras, 2004; Gomes, 2017).

3. Materials and methods

3.1. Materials

In this study, five clay samples (C6, Arb-11, AT-4, IGNIS and OL-400) supplied by EUROARCE®, Teruel, Spain, were investigated. These samples were sourced from different pits located within the Teruel province, specifically in the towns of Castellote, Estercuel, and Oliete. Prior to analysis, all samples were dried, sieved, and the analyses were conducted on fractions with particle sizes <150 μm.

3.2. Characterization of the samples

3.2.1. Mineralogical and chemical characterization

X-Ray diffraction (XRD) and X-Ray fluorescence (XRF) were used to quantify the mineral phases (identity and richness) of the samples. XRD analyses were performed by means of a diffractometer Philips®X-Pert, (Andover, USA) equipped with an automatic slit (CuKa, 4 to 70° 2Θ, 6/min, 40 kV). Data were analyzed using X-Powder software (Martín-Ramos, 2004). The main elements were determined by XRF using a Buker® S4 Pionner (Billerica, USA), with an X-ray Rh tube (60 kV, 150

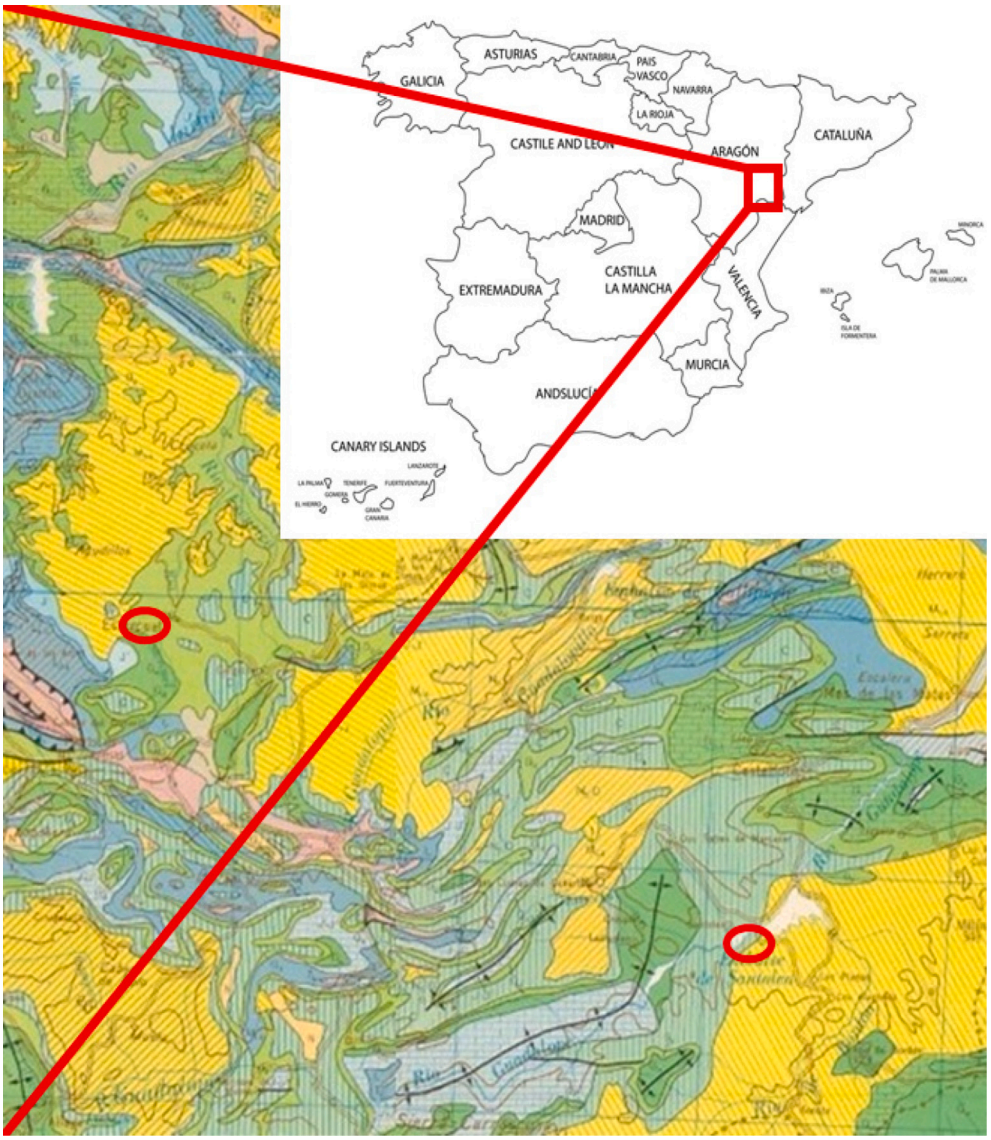

Fig. 1. Geology and location of the kaolinitic samples. Red circles indicate the location of the pists Fm. Utrillas (left) and Fm. Escucha (righ). (For interpretation of the references to colour in this figure legend, the reader is referred to the web version of this article.)

mA), controlled by software SpectraPlus (SpectraPLUS, LLC, Beaverton, USA). XRF accuracy was better than ±0.3% for major elements.

Semi-quantitative analysis was performed following Moore and Reynolds (1989) (Moore and Reynolds, 1989), and the final contents of the different mineral phases were calculated by combining XRD and chemical analytical data, following et al. (1994) (Torres-Ruíz et al., 1994) and López-Galindo et al. (1996) (López-Galindo et al., 1996).

3.2.2. Technological properties

Specific technological properties (determination of swelling capacity, apparent volume, and sedimentation capacity) were performed following the procedures described in the Spanish Pharmacopeia (RFE, 2015).

3.2.3. Scanning electron microscopy

Textural characteristics of the samples were analyzed through high resolution field emission Scanning Electron Microscopy (FESEM). The samples' characterization was carried out following the observations of secondary electron images (SE), in order to gather information about texture and chemical composition of the present minerals. For the analysis a Carl Zeiss GEMINI microscope (Carl Zeiss AG, Oberkochen, Germany) was used, equipped with an Oxford (EDX) sensor working at 5 kV.

3.3. Characterization of the disperse systems

3.3.1. Disperse systems preparation

Each clay sample was dispersed in purified water (final concentration 50% *w*/w) using a high velocity mixer (Heidolph®SilentCrusherM, Heidolph Instruments GmbH & Co. KG Schwabach, Germany) working at 8.000 rpm for 10 min.

3.3.2. Determination of pH and water content

The pH of the dispersed systems was measured using a pH-meter (Crison®, pH 25+, Crison Instruments, Barcelona, Spain), equipped with a semisolid sensor (5052 T). Six replicates were performed for each sample. The water content of all systems was measured by gravimetric technique: measuring the weight loss experienced by 1 g of each dispersed system. To do so, each sample was placed in an oven and the weight was monitored periodically until a constant weight was found. This experiment was performed in triplicate.

3.3.3. Rheological properties

Rheological study was carried out using a rotational viscosimeter (Thermo Scientific HAAKE®, RotoVisco 1, Thermo Fisher Scientific, Karlsruhe, Germany), equipped with a plate-plate geometry sensor (sensor Ø 20 mm serrated PP20/S) and connected to a computer equipped with HAAKE RheoWin® software (Thermo Fisher Scientific, Waltham, USA). The measurements were carried out at 25 °C working from 0 to 600 s^{-1} of shear rate. Rheological characterization includes flow curves and apparent viscosity of the studied samples. Six replicas were performed for each dispersed system studied.

3.3.4. Thermal properties

The study of the cooling kinetic of the different systems was done following the procedure described by Cara et al., 2000 (Cara et al., 2000). The final aim of this analysis is to evaluate the usefulness of the dispersed systems as potential thermal muds. A known amount of sample was placed in a cylindrical polyethylene terephthalate cell which was immersed in a thermostatic bath. Through a thermostatic probe located in the center of the cell, the temperature of the sample is measured in the range of 50 to 32 °C. This range was selected as the temperature range in which the dispersed system acts as a thermal mud. That is, the thermal mud is usually heated to 50–40 °C and subsequently applied over the skin until 32 °C (skin temperature). Since the human skin temperature is around 32 °C, once the thermal mud (dispersed system) reaches this temperature, no more heat exchange occurs, meaning the end of the thermal treatment. The experimental data obtained are fitted using Newton's law (Eq. (1)), which describes the heat transfer between two bodies in contact at different temperatures:

$$(T - T_{min}) = (T_{max} - T_{min}) \times e^{-Kt} \quad (1)$$

where, T is the sample temperature (°C) at time t (minutes), T_{min} is the ambient temperature (25 °C), T_{max} is the initial temperature (50 °C), and K is a constant which depends on the material and the device, given by the following Eq. (2):

$$K = \frac{P}{C} = \frac{P}{mCp} \quad (2)$$

Where P is an instrumental constant of the apparatus, C is the heat capacity of the sample, m is the weight of the sample used, and C_p is the specific heat. The instrumental constant was obtained using TiO_2 suspensions as a reference (Cara et al., 2000; Khiari et al., 2014).

3.3.5. Sun Protection factor

The determination of the Sun Protection Factor (SPF) was carried out through an *in-vitro* test proposed by Mansur et al., 1986 (Mansur et al., 1986). It is a method based on the measurement of absorbance in the range 290–320 nm. The SPF value is calculated with Eq. (3), using the aforementioned absorbance values. This method replaces the one proposed by Sayre et al., 1979 (Sayre et al., 1979). For this analysis, the solid phase (clays, 50% *w*/w) were dispersed in glycerin and purified water in equal parts (50:50 w/w). The reason for adding glycerin to the system is to keep them wet while the sample are exposed to the solar simulator and so, prevent them from drying.

Once the clay/water/glycerin dispersion were prepared, a small amount of sample (approximately 200–250 mg) was spread on a transparent methacrylate plate acting as a support. Subsequently, the samples were introduced inside the solar simulator, and irradiated for 1 h and a half, at an irradiance of 450 W/m^2. The selected irradiance corresponds to an irradiance slightly higher than that produced in one day in July in the south of Spain. To perform the absorbance measurement, 2–3 mg of the sample exposed in the solar simulator were taken and dispersed in 3 mL of ethanol (10 min under ultrasonic bath). An aliquot of 1.5 mL of the aforementioned dispersion was diluted in 1.5 mL of ethanol inside a 1 cm quartz cuvette. The measurement of the UV–vis spectrum was carried out in a Perkin-Elmer Lambda 365^+ spectrophotometer (PerkinElmer, Waltham, USA) from 290 to 310 nm (5 nm scan step). Mansur's mathematical Eq. (3) was used to calculate the SPF value of the studied samples:

$$SPF_{spectrophotometric} = CF \cdot \sum_{290}^{320} EE\,(\lambda) \cdot I(\lambda) \cdot Abs(\lambda) \quad (3)$$

Where *CF* is the correction factor (=10); *EE* is the erythematous effect of λ-wavelength radiation; *I* is the intensity of the solar spectrum, and *Abs* is the absorbance of wavelengths 290–320 nm. The values of (*EE (λ) and I(λ)*) are constants determined by Sayre et al., 1979 (see supplementary material) (Sayre et al., 1979). Applying the absorbance values obtained in the Mansur equation, the SPF values for the studied samples were calculated.

3.3.6. Stability of the preparations

The stability of the clay preparations was analyzed by transmittance and backscattering measurements in a TurbiscanLab (Formulaction, Toulouse, France). For that, 20 mL of the sample were placed in a glass which was scanned from bottom to top every 15 min for 48 h at 25 °C, recording the backscattering and transmittance of the samples. The stability of the dispersed systems was quantified from the data obtained by calculating their stability index (SI) using the following equations (Eqs. (4) and (5)):

$$SI(t) = \frac{1}{N_h} \sum_{t_i=1}^{t_{max}} \sum_{z_i=z_{min}}^{z_{max}} |BST(t_i, z_i) - BST(t_{i-1}, z_i)| \quad (4)$$

$$N_h = \frac{z_{max} - z_{min}}{\Delta h} \quad (5)$$

Where t_{max} is the time at which the SI is calculated; z_{min} and z_{max} are the lower and upper selected height limits, respectively; N_h is the number of height positions in the selected zone of the scan; Δh is the distance between measurement points in the scan of the vial, and *BST* is the signal at the time considered: transmittance (*T*) if it is >0.2% or backscattering (*BS*) otherwise (Vie et al., 2007; Ekosse and Nyembwe, 2012).

4. Results and discussion

4.1. Characterization of the samples

4.1.1. Mineralogical and chemical characterization

XRD patterns of the samples (Fig. 2) and XRF analysis (Table 1) were used to determine their mineralogical composition (Table 2). In view of the mineralogical results obtained, AT-4, IGNIS and OL-400 are formed mainly by phyllosilicates (illite (PDF 04–017-0519) and kaolinite (PDF 01–078-2110)), Arb-11 is formed by quartz (PDF 00–046-1045), and phyllosilicates. Finally, C6 is made up mainly of quartz. Traces (<5% *w*/w) of feldspars and interstratified clay minerals were also present in some samples. OL-400 is the richest sample in phyllosilicates (>90%), followed by IGNIS (>70%), AT-4 (>60%), Arb-11 (>50%) and C6 (>30%). Associated with these phyllosilicates, quartz was mostly detected, except for OL-400 with only 5% of this mineral, with C6 presenting the highest content (62%), followed by Arb-11 (39%), AT-4 (31%), and IGNIS (26%).

Special attention must be paid to the content of quartz, given that it has been classified by the International Agency for Research on Cancer (IARC) as a carcinogenic substance (IARC, 1997). Since we propose that these clays could be used for therapeutic and/or cosmetic purposes, at the time of making therapeutic sludge, its presence must be controlled and reduced as much as possible (López-Galindo and Viseras, 2004; Viseras et al., 2007; Khiari et al., 2014).

There is no specific limitation in terms of the maximum quartz content, but according to different studies carried out by Sánchez-Espejo et al. (2014); Khiari et al. (2014); Iannuccelli et al. (2016); Gutiérrez-

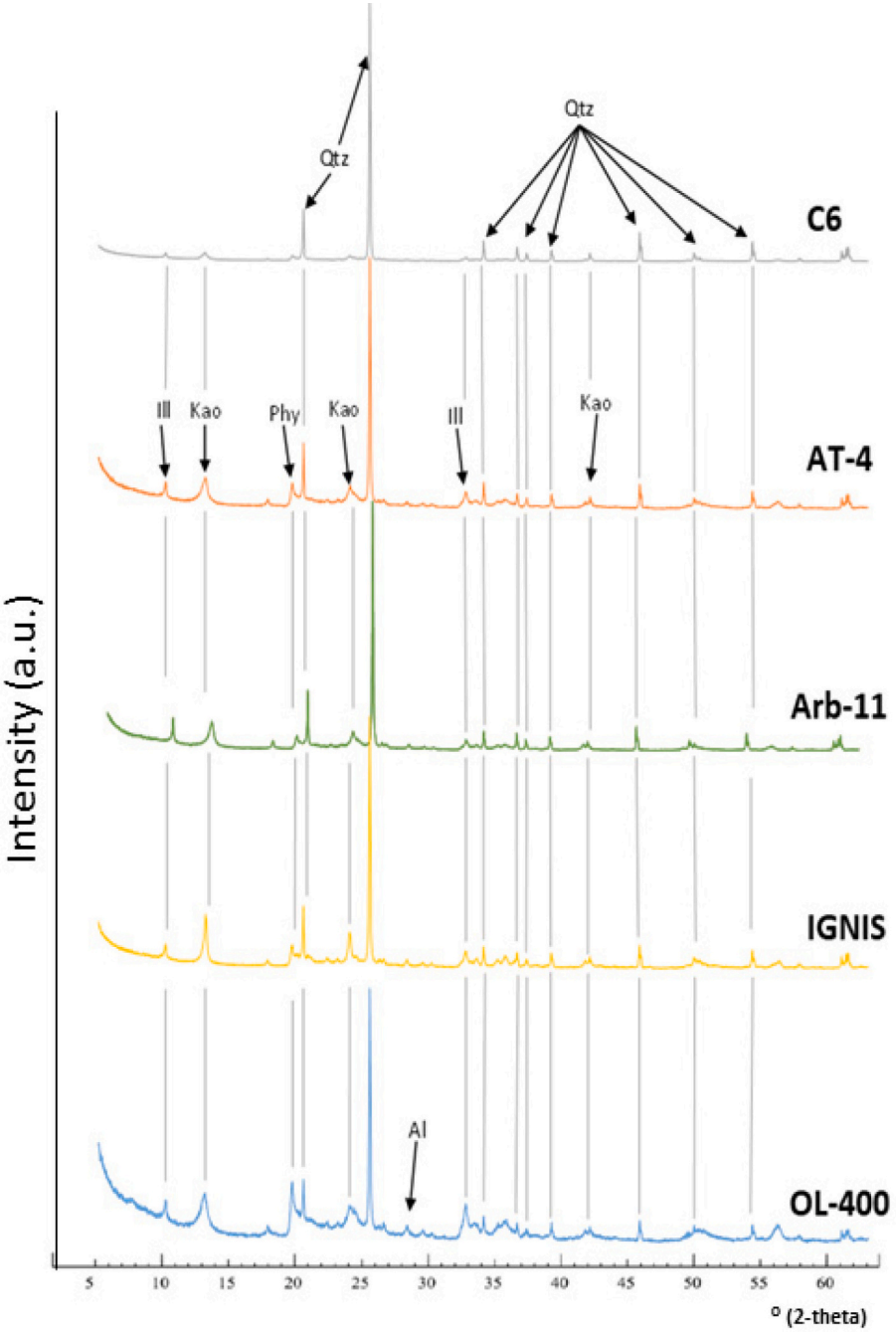

Fig. 2. XRD patterns of the studied bulk samples (Al: Alunite; Ill: Illite; KaoKaol: Kaolinite; Phy: Phyllosilicates; Qtz: Quartz).

Table 1
Chemical composition (major elements, % mass/mass) of the studied samples.

	C6	Arb-11	AT-4	IGNIS	OL-400
SiO_2	73.090	58.236	53.606	54.525	47.337
Al_2O_3	17.205	25.774	28.151	29.346	30.971
Fe_2O_3	1.130	1.776	1.995	1.743	2.501
MnO	0.008	0.009	0.011	0.013	0.005
MgO	0.166	0.378	0.405	0.456	0.527
CaO	0.037	0.224	0.234	0.208	0.341
Na_2O	0.118	0.162	0.156	0.146	0.198
K_2O	1.222	2.282	2.257	2.591	2.296
TiO_2	1.549	1.081	0.990	0.779	0.836
P_2O_5	0.046	0.096	0.062	0.070	0.060
LOI	4.850	9.400	11.62	9.710	14.230

Table 2
Mineralogical composition of the studied samples (% mass/mass).

	C6	Arb − 11	AT-4	IGNIS	OL-400
Kaolinite	22	34	43	46	70
Illite	13	23	22	26	21
Quartz	62	39	31	26	5

Mesías et al. (2017) and Mefteh and Medhioub (2021), it could be considered that less than ≤20% would be optimal (Khiari et al., 2014; Sánchez-Espejo et al., 2014; Iannuccelli et al., 2016; Gutiérrez Mesías et al., 2017; Mefteh and Medhioub, 2021).

4.1.2. Technological properties

Table 3 reveals that, following a 24-h period, all samples exhibited minimal swelling capacity. Specifically, C6, Arb-11, and AT-4 samples exhibited a sediment volume of 1 mL, while IGNIS and OL-400 samples displayed a sediment volume of 2 mL. This phenomenon can be attributed to the substantial presence of kaolinite and illite within the samples, both of which lack significant expansion properties. Furthermore, when considering the sedimentation capacities (SC) of the samples (ranging from 17 to 26 mL), Carr's Index (CI) (falling within the range of 24.32 to 25.22), and Hausner's Ratio (HR) (ranging from 1.32 to 1.34), it becomes evident that the fluidity of all samples is deemed satisfactory. These results signify robust flow properties, which hold the potential for further enhancement through the introduction of lubricating agents. Lastly, the sedimentation volume test elucidated that only the IGNIS sample conformed to pharmacopeial requirements.

4.1.3. Scanning electron microscopy

SEM images (Fig. 3) revealed that the samples consist of a mixture of phyllosilicates (kaolinite and illite), along with quartz and occasional occurrences of anhydrite and alunite. Kaolinite is observed in arb-11 as subhedral to anhedral crystals with a hexagonal or pseudo-hexagonal morphology and irregular edges (Fig. 3A). Euhedral to subhedral crystals with a hexagonal contour were observed in sample C6 (Fig. 3B), as well as "book" type aggregates in sample AT-4 (Fig. 3C) (Dixon, 1989; Galán, 2006; Lagaly et al., 2006). In this sample, illite appeared as nanometric crystals ranging from subhedral to anhedral, with a planar habit. These crystals can be found in the form of aggregates arranged along the c-axis (Fig. 3D). Occasionally, they may appear as subhedral to anhedral crystals with a planar habit and pseudo-hexagonal outline (Inoue and Kitagawa, 1994).

In addition, the association of quartz with the samples was confirmed by the quartz grains, characterized by their straight edges and smooth faces (Vos et al., 2014; Mejía-Ledezma et al., 2020), as observed in sample OT-4 (Fig. 3D). Apart from the mineral phases described above, which are observed in all samples, there are two mineral phases that are only present in one of them. In the OL-400 sample, alunite and anhydrite were detected. Alunite appears as euhedral to subhedral crystals with a rhombohedral shape (Fig. 3E), which are covered by small plates of both illite and kaolinite (Dill, 2001). Anhydrite is observed as anhedral prismatic crystals, characterized by a banded appearance (Fig. 3E) (Yuan et al., 2013; Tang et al., 2016, 2022; Hou et al., 2022).

The morphology of the mineral phases varies with the mineral content in the successive samples. Sample C6, which has the lowest content of phyllosilicates, exhibits the most crystalline morphology of the mineral phases. Conversely, in sample OL-400, despite having the highest content of phyllosilicates, the mineral phases exhibit a less crystalline morphology. Additionally, alteration products such as anhydrite and alunite can be observed in the OL-400 sample. Therefore, it can be confirmed that as the content of phyllosilicates increases, the morphologies of the mineral phases become more altered.

Table 3
Technological properties of clay samples were assessed based on sediment volume in the swelling test, uncompacted bulk density (UBD), compacted bulk density (CBD), sedimentation capacity (SC), Carr's index (CI), Hausner's ratio (HR), and sedimentation volume.

	C6	Arb-11	AT-4	IGNIS	OL-400
Swelling test (mL)	1.00	1.00	1.00	2.00	2.00
UBD (g/mL)	0.98	0.90	0.87	0.76	0.82
CBD (g/ml)	1.30	1.19	1.16	1.01	1.09
SC (mL)	17.00	21.00	22.00	26.00	24.00
CI (%)	24.51	24.32	25.22	25.00	24.59
HR	1.32	1.32	1.34	1.33	1.33
Sedimentation volume (mL)	> 2.00	> 2.00	> 2.00	< 2.00	> 2.00

4.2. Characterization of the disperse systems

4.2.1. Determination of pH and water content

All the dispersed systems exhibited a water content of approximately 50%, which is close to the theoretical value, confirming their proper preparation and handling. In terms of pH (Table 4), the systems showed values ranging from 3.37 to 3.97, indicating a slightly acidic nature. However, the IGNIS sample deviated from this trend with a pH value of 7.24, closer to neutral. Overall, all the systems fell within the acceptable pH range for topical application on the skin surface (Lukić et al., 2021).

4.2.2. Rheological properties

The flow curves of the dispersed systems exhibit non-Newtonian behavior, characterized by either anti-thixotropic or rheopectic properties (Fig. 4). This implies that the viscosity of the systems increases as the applied stress rises. Such rheopectic behavior is commonly observed in systems in case of 1:1 phyllosilicates and at high concentrations (Viseras et al., 2007). One of the most important rheological properties for a clay-based system intended for skin application is its apparent viscosity. It is crucial for the system to possess an appropriate viscosity to ensure that it remains on the site of application during treatment. Adequate consistency and viscosity provide the system with good plasticity and skin adherence.

Apparent viscosity values were determined from the experimental data at a shear rate of 250 s^{-1} (Table 4). Among the samples, OL-400 exhibited the highest viscosity of 1.5 Pa·s, while C6 had the lowest viscosity of 0.21 Pa·s. These values correspond to the phyllosilicate content in each sample, with OL-400 having a higher content (91%) and C6 having a lower content (22%). The Arb-11 and IGNIS samples displayed intermediate and similar apparent viscosity values (0.34 Pa·s and 0.39 Pa·s, respectively), indicating similar rheological behavior. These findings demonstrate that the apparent viscosity increases with the phyllosilicate content in the samples.

4.2.3. Thermal properties

Experimental and theoretical specific heats, along with the temperature of the dispersed systems after 20 min of their application and the time required for them to reach 32 °C, are shown in Table 5. All systems presented similar experimental specific heat values, in the range of 2.72 to 2.83 J/gK, a value that is independent of the composition of the solid phase. Experimental specific heat values (Cp_{exp}) were somewhat larger than those of theoretical specific heat values (Cp_{theo}), and similar to those measured in other analogous systems by other authors (Legido et al., 2007; Viseras et al., 2007; Khiari et al., 2014; Sánchez-Espejo et al., 2015; Mato et al., 2017; Awad et al., 2018; Barhoumi et al., 2019). Many of the works have shown that the specific heat of the systems depends mainly on the water content and to a lesser extent on the composition of the solid phase.

The most interesting thermal properties are the temperature after the contact time corresponding to the application of the thermal muds (20 min, T_{20min}) and the time it takes for the system to reach the temperature of the skin (32 °C, $t_{32\ °C}$), when the heat transfer stops. The samples presented T_{20min} values between 33.9 and 34.6 °C and $t_{32\ °C}$ values between 24 and 26 min. In view of the results, the system made with the Arb-11 sample is the one that took the longest to cool down, reaching 32 °C in 26.22 min. It also had the highest temperature after the application time (34.62 min), while the preparation with sample AT-4 was the one that cooled the fastest (24.3 min) and presented the lowest temperature after 20 min (33.89 °C).

Therefore, it can be stated that all the dispersed systems prepared had adequate thermal properties, guaranteeing heat transfer between them and the skin during application, considering the typical procedure of thermal muds application.

4.2.4. Determination of the Sun Protection factor (SPF)

Assessing the Sun Protection Factor (SPF) is crucial in determining a

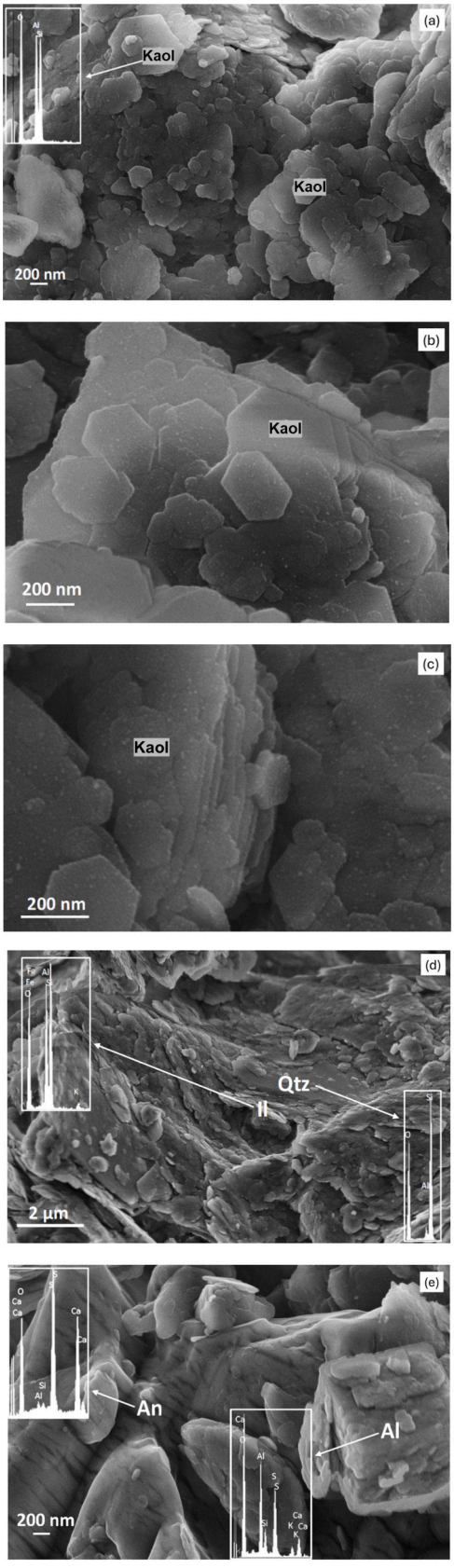

(caption on next column)

Fig. 3. Microphotographs of the studied samples, showing their typical textures, and chemical analysis of each mineral phase. A: Kaolinite crystals, from subhedral to allotriomorfic pseudo-hexagonal morphology and irregular contour (sample arb-11). B: Kaolinite crystals, from euhedral to subhedral with hexagonal morphology (sample C6). C: Aggregates type "book" of kaolinite (sample AT-4). D: Illite crystals, from subhedral to allotriomorfic, with planar habit and crystals of quartz witch smooth shape (sample AT-4). E: Allotriomorfic to subhedral prismatic anhydrite crystals and euhedral to subhedral romboedric crystals of alunite (sample OL-400). (An: Anhydrite; Al: Alunite; Ill: Illite; Kaol: Kaolinite; Qtz: Quartz).

product's capability to shield against ultraviolet B (UVB) radiation. SPF quantifies the necessary UV radiation dosage to induce a minimal erythema dose (MED) on safeguarded skin relative to skin without protection. This metric is instrumental in evaluating sunscreen's effectiveness, as it denotes how long human skin can be exposed to solar UV radiation without incurring sunburn. SPF is not merely a measure to avert sunburn but is pivotal in mitigating skin cancer risks and curtailing premature skin aging. For instance, a sunscreen with an SPF of 15 implies that it permits 15 times longer sun exposure compared to unprotected skin. The American Academy of Dermatology advocates for a minimum SPF of 15 in sunscreens for robust protection against UV radiation. Hence, the importance of SPF in dermo-cosmetic products is paramount, serving as a fundamental defense against the adverse effects of UV exposure, such as sunburn, skin aging, and skin cancer (Dutra et al., 2004; Begoun, 2009; Kaur and Saraf, 2010; Mbanga et al., 2014; Gutiérrez Mesías et al., 2017; Zayd et al., 2019).

All systems were then evaluated through UV–vis spectrophotometry applying Eq.3 (Mansur et al., 1986). It is worth to highlight that the dispersed systems analyzed only differ in the mineralogical composition of the solid phase, having all of them the same liquid phase and the same solid concentration (50% *w*/w).

In view of the SPF results obtained (Fig. 5, SM2 and SM3), it can be observed that, in all the samples, there is an increase in the SPF value until reaching one hour of exposure, moment from which the value begins to decrease.

The average SPF values obtained (7.46, 11.57, 14.49, 12.05, and 16.65 for C6, Arb-11, AT-4, IGNIS, and OL-400, respectively) also correlates with the amount of phyllosilicates. In fact, the lowest average SPF value belongs to C6 sample, the one with the lowest phyllosilicates content, while the sample with the highest SPF value (OL-400) reported the highest phyllosilicates percentage.

The SPF value provides an estimate of the amount of time that the human skin can be exposed to the sun without experiencing sunburn. Therefore, with the C6 sample, the maximum time exposure is approximately 7.46 times longer without producing skin redness. On the other hand, the OL-400 sample provide protection for 16.65 times longer. For example, if a person's skin would typically burn after 10 min of sun exposure without sunscreen (something that depends on the skin type or "phototype"), the C6 sample would provide protection for approximately 75 min, and the OL-400 sample would provide protection for 167 min without any skin redness.

As shown in Fig. 5, the SPF values are not constant over time, but vary as solar radiation exposure increases. The highest protection occurs after 60 min of exposure, with values of 9.92 for the C6 sample, 13.54 for Arb-11, 16.73 for AT-4, 16.47 for IGNIS, and 22.53 for OL-400 (Fig. 5). After this point, the dispersed systems begin to lose effectiveness in protecting against UV B radiation.

The American Academy of Dermatology (AAD) recommends the daily use of sunscreen with a minimum SPF of 15. In this regard, the disperse system formulated with OL-400 would be the only one that meets this requirement.

4.2.5. *Stability of the preparations*

The stability of the preparations was evaluated by analyzing the sedimentation of the suspended particles by combined measurements of

Table 4
pH (mean values ± s.d.; $n = 6$) and apparent viscosity (250 s^{-1}, 25 °C) (mean values ± s.d.; n = 6) of the dispersed systems.

	pH ± s.d.	η (Pa·s) ± s.d.
C6	3.37 ± 0.02	0.21 ± 0.02
Arb-11	3.62 ± 0.02	0.34 ± 0.02
IGNIS	7.24 ± 0.03	0.39 ± 0.03
AT-4	3.41 ± 0.02	0.59 ± 0.05
OL-400	3.97 ± 0.05	1.50 ± 0.10

backscattering and transmittance of the samples placed in a glass vial. From these measurements, a stability index (SI) was obtained (Fig. 6). The first read was used as a reference, so for $t = 0$, a value of SI = 0 was considered.

A suspension of particles is normally considered stable when the SI < 2 (Vie et al., 2007; Ekosse and Nyembwe, 2012). As it can be observed in Fig. 6, the dispersion C6 only met this criterion for 3 h, and after that time its SI exceeded 2. On the contrary, the rest of the preparations were remarkably stable: Arb-11 took 26 h after its preparation to reach a SI of 2, IGNIS after 33.75 h, and AT-4 after 41 h. The OL-400 preparation was the most stable and did not surpass the threshold of SI = 2 during the 45 h of the stability measurement.

The phenomenon of destabilization of the aforementioned systems can be observed. In the preparations with samples C6, Arb-11, AT-4, and IGNIS, the sedimentation of the suspended particles is evident through the separation of phases, indicated by clarification in the upper part of the sample. However, in the dispersed system prepared with the OL-400 sample, which is stable as mentioned earlier, no formation of a water layer was visible during the analysis period.

In the context of the results obtained in this study, kaolinite's structural and compositional attributes significantly contribute to its efficacy in dermatological and pharmaceutical formulations. As a hydrated aluminum silicate, kaolinite is structured in a 1:1 layering of one tetrahedral silica sheet coupled with one octahedral alumina sheet. This distinctive arrangement not only enhances its physical stability but also imparts critical functional properties such as high UV radiation absorption and superior thermal insulation, which are essential for effective sun protection formulations (López-Galindo et al., 2007).

The research findings from Hoang-Minh et al. (2010) (Hoang-Minh et al., 2010) provide substantial verification of kaolinite's robust UV-blocking capabilities, mainly due to its ability to efficiently reflect and scatter ultraviolet light. This feature stems from its platy particle morphology. This characteristic is particularly advantageous, making kaolinite an ideal component in sunscreen products by establishing a formidable physical barrier against UV radiation. The practical implications are evident in the enhanced UV protection observed in the sunscreen formulations tested, underscoring the mineral's potential in sun care products. The recent review by Sarruf et al. (2024) (Sarruf et al., 2024) further supports this, indicating the widespread use of kaolinite for its physiochemical properties, contributing to sunscreen and dermatological treatments.

Additionally, kaolinite's low thermal conductivity positions it as a prime candidate for therapeutic thermal mud applications. When used in such contexts, kaolinite facilitates a slow and controlled heat release, allowing for extended thermal treatments. This gradual heat release can significantly augment therapeutic efficacy, providing sustained benefits in thermal therapy settings (Carretero et al., 2006a, 2006b).

These properties underscore kaolinite's versatility in pharmaceutical and dermatological applications, leveraging its unique mineralogical features for enhanced product performance (Bergaya and Lagaly, 2013). Integrating kaolinite into these products enhances their functionality and highlights the potential of mineral-based ingredients in advancing current formulation technologies. This discussion aligns with the observed data and suggests broader implications for incorporating kaolinite in diverse application areas.

Table 5
Specific heats (Cp), theoretical (theo) and experimental (exp) values, time (t) required to reach 32 °C and temperature (T) after 20 min of application of the studied dispersed systems.

	Cp_{theo} (J/gK)	Cp_{exp} (J/gK)	$t_{32\ °C}$ (min)	T_{20min} (°C)
C6	2.40	2.78	25.38	34.28
Arb-11	2.60	2.72	26.22	34.62
IGNIS	2.60	2.81	25.67	34.40
AT-4	2.70	2.72	24.30	33.89
OL-400	2.72	2.83	25.75	34.39

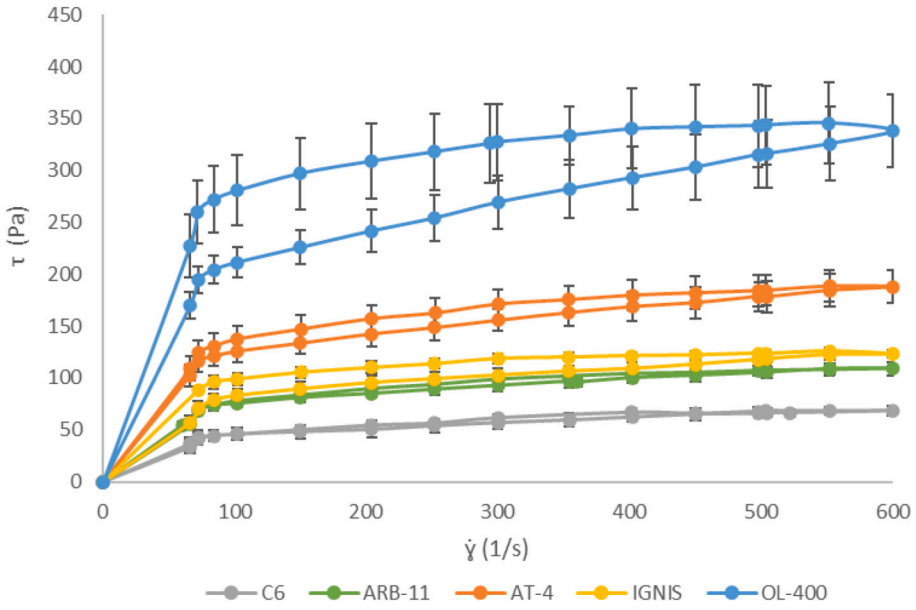

Fig. 4. Flow curves of dispersed systems, shear rate *vs* shear stress. Red arrows over the curves indicate the direction. (For interpretation of the references to colour in this figure legend, the reader is referred to the web version of this article.)

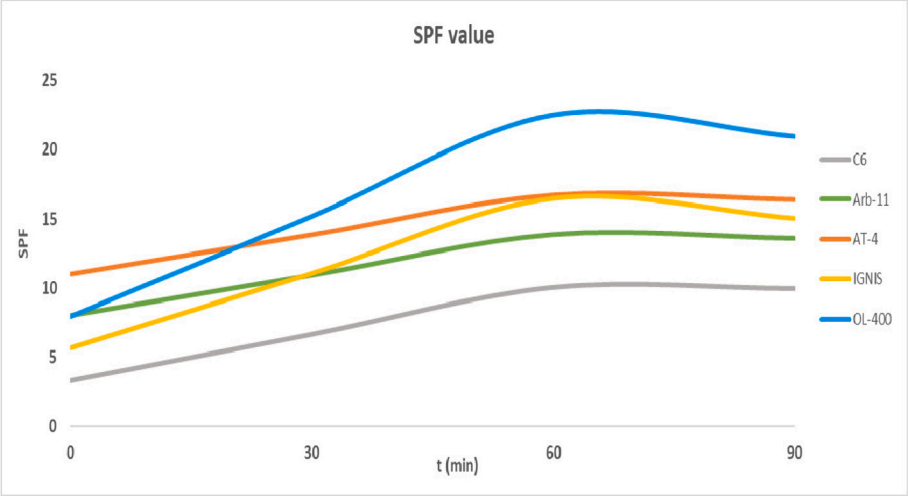

Fig. 5. Variation of the SPF value of the analyzed samples (see in supplementary material 2 the SPF value labeled of the disperse systems using the method developed by Mansur et al. (1986) (Mansur et al., 1986).

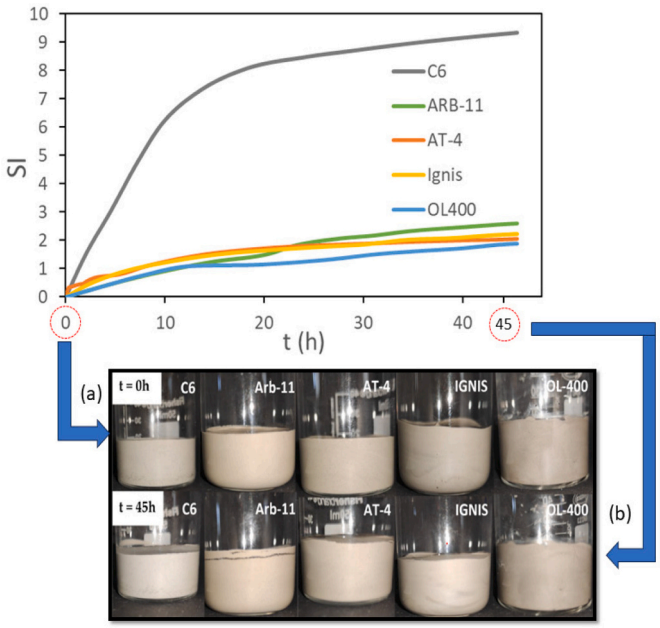

Fig. 6. Stability Index (SI) of the preparations incubated at 25 °C conducted over a period of 45 h. The photos of the samples depict a comparison immediately before commencing the measurements (a) and at the conclusion of the 45-h analysis (b), where the clarification process can be observed.

5. Conclusions

In this study, five clay minerals samples extracted from different pits in the province of Teruel (Spain) have been evaluated from a pharmaceutical and cosmetic point of view. In particular, the final aim was to discern the potential of these samples to be used as thermal muds and/or sun protection products, apart from their already common use in ceramics. The samples studied, except for sample C6, primarily consist of kaolinite and illite (classified as clay minerals). Samples OL-400 and IGNIS can be classified as high purity clays, while samples AT-4 and Arb-11 are mixtures of clays, and sample C6 is a kaolinite sand. The crystalline silica (quartz) content is higher than 20% in all samples except for OL-400, suggesting the need for treatment to reduce it before handling. The textural analysis reveals that as the content of phyllosilicates increases, their morphology becomes more altered. After their dispersion in aqueous solution, the pH of the systems falls within the range of the skin's pH, meaning that they could be safely used as topical formulations. Rheologically, the systems exhibit typical non-Newtonian flow curves, displaying anti-thixotropic behavior and suitable apparent viscosity for topical application. The study of thermal properties revealed similar results, in agreement with the fact that the specific heat of the systems highly depends on the water content rather than the composition of the solid phase. The temperature values after 20 min (considered the minimum application time) and the time required to reach 32 °C (skin temperature) ensure effective heat transfer between the system and the skin during application, making them suitable for use as thermotherapeutic agents.

In terms of SPF, as the phyllosilicates content increased, the value also increased until reaching one hour of exposure, after which it started to decrease. Most samples exhibited an SPF >10. Furthermore, the majority of samples demonstrated remarkable stability, except for sample C6. The OL-400 sample stood out as the most stable, not suffering from phase separation. In view of these results, it can be concluded that all samples, except for C6, are suitable as raw materials for the preparation of therapeutic muds in balneotherapy. Additionally, they have potential as ingredients in sun protection products, with OL-400 exhibiting the highest potential due to its high purity. It cannot be forgotten, therefore, that further purification steps to reduce the amount of associated phases (like quartz) would increase even more their exploitability as cosmetic excipients in the formulation of more specific dosage forms. In any case, the present study brings added value to Spanish natural resources, opening a new range of possibilities to exploit.

Funding

This work was supported by the spanish project PID2022-137603O13-100 of the Ministerio de Ciencia, Innovación y Universidades. R.d.M.B. wishes to acknowledge by EMERGIA, Junta de Andalucía, Universidad de Sevilla, Spain,Contract number USE 23922-W.

CRediT authorship contribution statement

Ismael Monterde Cortés: Writing – original draft, Project administration, Methodology, Investigation, Data curation, Conceptualization. **Raquel de Melo Barbosa:** Writing – review & editing, Writing – original draft, Supervision, Project administration, Methodology. **Fátima García-Villén:** Writing – review & editing, Supervision, Data curation.

Ignacio Moya Ramírez: Project administration, Methodology, Data curation. **Marina Massaro:** Writing – original draft, Data curation. **Serena Riela:** Investigation, Conceptualization. **Alberto López-Galindo:** Writing – review & editing, Supervision. **César Viseras:** Writing – review & editing, Supervision, Investigation, Conceptualization. **Rita Sánchez-Espejo:** Writing – review & editing, Supervision, Investigation, Conceptualization.

Declaration of competing interest

All authors declare that they have no conflicts of interest.

Data availability

No data was used for the research described in the article.

Appendix A. Supplementary data

Supplementary data to this article can be found online at https://doi.org/10.1016/j.clay.2024.107422.

References

Aguilar, M.J., Ramirez del Pozo, J., Riba, O., 1971. Algunas precisiones sobre la sedimentación y paleoecología del cretácico inferior de la zona de Utrillas-Villarroya de los Pinares (Teruel). Estud. Geol. 27, 497–512.

Ataytür, Ö., Gautheron, C., Horbe, A., Allard, T., 2024. Thermal stability of artificial radiation-induced defects in kaolinite: Enhancing EPR dating protocol. Appl. Clay Sci. 252, 107349 https://doi.org/10.1016/j.clay.2024.107349.

Awad, M.E., López-Galindo, A., El-Rahmany, M.M., El-Desoky, H.M., Viseras, C., 2017a. Characterization of Egyptian kaolins for health-care uses. Appl. Clay Sci. 135, 176–189. https://doi.org/10.1016/j.clay.2016.09.018.

Awad, M.E., López-Galindo, A., Setti, M., El-Rahmany, M.M.M., Iborra, C., 2017b. Kaolinite in pharmaceutics and biomedicine. Int. J. Pharm. 533, 34–48. https://doi.org/10.1016/j.ijpharm.2017.09.056.

Awad, M.E., López-Galindo, A., Sánchez-Espejo, R., El-Rahmany, M.M., Viseras, C., 2018. Thermal properties of some Egyptian kaolin pastes for pelotherapeutic applications: Influence of particle geometry on thermal dosage release. Appl. Clay Sci. 160, 193–200. https://doi.org/10.1016/j.clay.2017.11.005.

Barhoumi, T., Bekri-Abbes, I., Srasra, E., 2019. Physicochemical characteristics and suitability of curative pastes made of Tunisian clay minerals and thermal waters for use in pelotherapy. C. R. Chim. 22, 126–131. https://doi.org/10.1016/j.crci.2018.11.006.

Bartolomé, J.F., 1997. El caolín: composición, estructura, génesis y aplicaciones. Bol. Soc. Española Cerám. Vidrio 36, 7–19.

Begoun, P., 2009. The Original Beauty Bible. Beginning Press, Renton, Washington.

Bergaya, F., Lagaly, G., 2013. General Introduction: Clays, clay minerals, and clay Science. In: Bergaya, F., Lagaly, G. (Eds.), Handbook of Clay Science. Elsevier, Amsterdam, pp. 1–19. https://doi.org/10.1016/B978-0-08-098258-8.00001-8.

Brigatti, M.F., Galan, E., Theng, B.K.G., 2013. Structures and Mineralogy of Clay Minerals. In: Bergaya, F., Theng, B.K.G., Lagaly, G. (Eds.), Handbook of Clay Science. Developments in Clay Science. Elsevier Ltd., Amsterdam, pp. 21–81. https://doi.org/10.1016/S1572-4352(05)01002-0.

Cara, S., Carcangiu, G., Padalino, G., Palomba, M., Tamanini, M., 2000. The bentonites in pelotherapy: thermal properties of clay pastes from Sardinia (Italy). Appl. Clay Sci. 16, 125–132.

Carretero, M.I., 2002. Clay minerals and their beneficial effects upon human health. A review. Appl. Clay Sci. 21, 155–163.

Carretero, M.I., 2020. Clays in pelotherapy. A review. Part II: Organic compounds, microbiology and medical applications. Appl. Clay Sci. 189, 105531 https://doi.org/10.1016/j.clay.2020.105531.

Carretero, M.I., Pozo, M., 2010. Clay and non-clay minerals in the pharmaceutical and cosmetic industries Part II. Active ingredients. Appl. Clay Sci. 47, 171–181. https://doi.org/10.1016/j.clay.2009.10.016.

Carretero, M.I., Gomes, C.S.F., Tateo, F., 2006a. Chapter 11.5 Clays and human health. In: Developments in Clay Science, pp. 717–741. https://doi.org/10.1016/S1572-4352(05)01024-X.

Carretero, M.I., Gomes, C.S.F., Tateo, F., 2006b. Clays and human health. In: Bergaya, F., Theng, B.K.G., Lagaly, G. (Eds.), Handbook of Clay Science. Developments in Clay Science. Elsevier Ltd., Amsterdam, pp. 717–741. https://doi.org/10.1016/S1572-4352(05)01024-X.

Cervera, A., Pardo, G., Villena, J., 1976. Algunas precisiones litoestratigráficas sobre la formación "Lignitos de Escucha". Tecniterrae 14, 25–33.

Chumakov, N.M., Zharkov, M.A., Herman, A.B., Doludenko, M.P., Kalandadze, N.N., Lebedev, E.L., Ponomarenko, A.G., Rautian, A.S., 1995. Climatics belts of the Mid-cretaceous time. Stratigr. Geol. Correl. 3, 241–260.

Dill, H.G., 2001. The geology of aluminium phosphates and sulphates of the alunite group minerals: a review. Earth Sci. Rev. 53, 35–93. https://doi.org/10.1016/S0012-8252(00)00035-0.

Dixon, J.B., 1989. Kaolin and serpentine group minerals. In: Dixon, J.B., Weed, S.B. (Eds.), Minerals in Soil Environments. Soil Science Society of America, Madison, WI, pp. 467–525.

Dutra, E.A., Gonçalves Da Costa, E., Oliveira, D.A., Kedor-Hackmann, E.R.M., Miritello Santoro, M.I.R., 2004. Determination of sun protection factor (SPF) of sunscreens by ultraviolet spectrophotometry. Braz. J. Pharm. Sci. 40, 381–385. https://doi.org/10.1590/S1516-93322004000300014.

Ekosse, G.A., Nyembwe, T.M., 2012. Effects of temperature and pH on sedimentation behaviour of kaolinite suspensions. J. Dispers. Sci. Technol. 33, 63–70.

Galán, E., 2006. Genesis of clay minerals. In: Bergaya, F., Theng, B.K.G., Lagaly, G. (Eds.), Handbook of Clay Science. Developments in Clay Science. Elsevier, Ltd, Amsterdam, pp. 1129–1162. https://doi.org/10.1016/S1572-4352(05)01042-1.

Gomes, C.S.F., 2017. Healing and edible clays: a review of basic concepts, benefits and risks. Environ. Geochem. Health 1739–1765. https://doi.org/10.1007/s10653-016-9903-4.

Guimerá, J., 1984. Palaeogene evolution of deformation in the northeastern Iberian Peninsula. Geol. Mag. 121, 413–420. https://doi.org/10.1017/S0016756800029940.

Gutiérrez Mesías, L.G., Romero Qwisgaard, A.M., Chávez Untiveros, G.P., Palomino Kobayashi, L.A., Moromisato Shimabukuro, L.E., Kitazono Sugahara, A.A., 2017. Comparison of the photoprotective effects of sunscreens using spectrophotometric measurements or the survivability of yeast cells exposed to UV radiation. Rev. Soc. Quím. Perú 83, 294–307.

Hernández, A.C., Sánchez-Espejo, R., Meléndez, W., González, G., López-Galindo, A., Viseras, C., 2019. Characterization of Venezuelan kaolins as health care ingredients. Appl. Clay Sci. 175, 30–39. https://doi.org/10.1016/j.clay.2019.01.003.

Hoang-Minh, T., Le, T.L., Kasbohm, J., Gieré, R., 2010. UV-protection characteristics of some clays. Appl. Clay Sci. 48, 349–357. https://doi.org/10.1016/j.clay.2010.01.005.

Hou, C., Jin, X., He, J., Li, H., 2022. Experimental studies on the pore structure and mechanical properties of anhydrite rock under freeze-thaw cycles. JRMGE 14, 781–797. https://doi.org/10.1016/j.jrmge.2021.10.005.

Iannuccelli, V., Maretti, E., Sacchetti, F., Romagnoli, M., Bellini, A., Truzzi, E., Miselli, P., Leo, E., 2016. Characterization of natural clays from Italian deposits with focus on elemental composition and exchange estimated by EDX analysis: potential pharmaceutical and cosmetic uses. Clay Clay Miner. 64, 719–731. https://doi.org/10.1346/CCMN.2016.064038.

IARC, 1997. Silica, some silicates, coal dust and Para-Aramid Fibrils. In: Monographs on the Evaluation of Carcinogenic Risks to Humans. International Agency for Research on Cancer, World Health Organization, France.

Inoue, A., Kitagawa, R., 1994. Morphological characteristics of illitic clay minerals from a hydrothermal system. Am. Mineral. 79, 700–711.

Kaur, C.D., Saraf, S., 2010. In vitro sun protection factor determination of herbal oils used in cosmetics. Pharm. Res. 2, 22–25. https://doi.org/10.4103/0974-8490.60586.

Khiari, I., Mefteh, S., Sánchez-Espejo, R., Cerezo, P., Aguzzi, C., López-Galindo, A., Jamoussi, F., Viseras Iborra, C., 2014. Study of traditional Tunisian medina clays used in therapeutic and cosmetic mud-packs. Appl. Clay Sci. 101, 141–148. https://doi.org/10.1016/j.clay.2014.07.029.

Lagaly, G., Ogawa, M., Dékány, I., 2006. Clay Mineral Organic Interactions. In: Bergaya, F., Theng, B.K.G., Lagaly, G. (Eds.), Handbook of Clay Science. Developments in Clay Science. Elsevier Ltd., Amsterdam, pp. 309–377. https://doi.org/10.1016/S1572-4352(05)01010-X.

Legido, J.L., Medina, C., Mourelle, M.L., Carretero, M.I., Pozo, M., 2007. Comparative study of the cooling rates of bentonite, sepiolite and common clays for their use in pelotherapy. Appl. Clay Sci. 36, 148–160. https://doi.org/10.1016/j.clay.2006.06.014.

López-Galindo, A., Viseras, C., 2004. Pharmaceutical and cosmetic applications of clays. In: Wypych, F., Satyanarayana, K.G. (Eds.), Clay Surfaces: Fundamentals and Applications. Elsevier Ltd., Amsterdam, pp. 268–289.

López-Galindo, A., Torres Ruiz, J., González-López, J.M., 1996. Mineral quantification in sepiolite-palygorskite deposits using X-ray diffraction and chemical data. Clay Miner. 31, 217–225.

López-Galindo, A., Viseras, C., Cerezo, P., 2007. Compositional, technical and safety specifications of clays to be used as pharmaceutical and cosmetic products. Appl. Clay Sci. 36, 51–63. https://doi.org/10.1016/j.clay.2006.06.016.

López-Galindo, A., Viseras, C., Aguzzi, C., Cerezo, P., 2011. Pharmaceutical and cosmetic uses of fibrous clays. In: Galán, E., Singer, A. (Eds.), Developments in Clay Science. Elsevier B.V, Amsterdam, pp. 299–324. https://doi.org/10.1016/B978-0-444-53607-5.00013-X.

Lukić, M., Pantelić, I., Savić, S.D., 2021. Towards optimal ph of the skin and topical formulations: from the current state of the art to tailored products. Cosmetics 8, 1–18. https://doi.org/10.3390/cosmetics8030069.

Mansur, J.S., Breder, M.N.R., Mansur, M.C.A., Azulay, R.D., 1986. Determinação do fator de proteção solar por espectrofotometria. An. Bras. Dermatol. Rio De Janeiro 61, 121–124.

Martín-Ramos, J.D., 2004. X-powder, a software package for powder X-ray diffraction analysis, [WWW Document]. URL Legal Deposit G.R.1001/04, available at. http://www.xpowder.com.

Mato, M.M., Casás, L.M., Legido, J.L., Gómez, C., Mourelle, L., Bessières, D., Plantier, F., 2017. Specific heat of mixtures of kaolin with sea water or distilled water for their use in thermotherapy. J. Therm. Anal. Calorim. 130, 479–484. https://doi.org/10.1007/s10973-017-6227-2.

Mbanga, L., Mulenga, M., Mpiana, P.T., Bokolo, K., Mumbwa, M., Mvingu, K., 2014. Determination of sun protection factor (SPF) of some body creams and lotions

marketed in Kinshasa by ultraviolet spectrophotometry. Int. J. Adv. Res. Chem. Sci. (IJARCS) 1, 7–13.
Mefteh, S., Medhioub, M., 2021. Composition, quality, and certification of some Tunisian thermal muds used in pelotherapy. Arab. J. Geosci. 14, 2140. https://doi.org/10.1007/s12517-021-08532-y.
Mejía-Ledezma, R.O., Kasper-Zubillaga, J.J., Alvarez-Sánchez, L.F., Mendieta-Lora, M., Arellano-Torres, E., Tetlalmatzi-Martínez, J.L., Gonzalez-Bermúdez, A., Patiño-Andrade, D., Armstrong-Altring, J.S., 2020. Surface textures of quartz and ilmenite grains from dune and beach sands of the Gulf of Mexico Coast, Mexico: Implications for fluvial, aeolian and marine transport. Aeolian Res. 45, 100611 https://doi.org/10.1016/j.aeolia.2020.100611.
Meléndez, N., Liesa, C.L., Soria, A.R., Meléndez, A., 2009. Lacustrine system evolution during early rifting: El Castellar Formation (Galve sub-basin, Central Iberian Chain). Sediment. Geol. 222, 64–77. https://doi.org/10.1016/j.sedgeo.2009.05.019.
Moore, D.M., Reynolds, R.C., 1989. X-Ray Diffraction and the Identification and Analysis of Clay Minerals. Oxford University Press, New York.
Murray, H.H., 2000. Traditional and new applications for kaolin, smectite, and palygorskite: a general overview. Appl. Clay Sci. 17, 207–221. https://doi.org/10.1016/S0169-1317(00)00016-8.
Pardo, G., 1979. Estratigrafía y sedimentología de las formaciones detríticas del cretácico inferior terminal del bajo Aragón Turolense. Universidad de Zaragoza, Zaragoza.
Perea, M.A., 2014. Historia de la peloterapia. In: Hernández Torres, A. (Ed.), Peloterapia: Aplicaciones Médicas y Cosméticas de Fangos Termales. Fundación para la Investigación e Innovación en Hidrología Médica y Balneoterapia "Bílbilis", Madrid, pp. 47–53.
Querol, X., 1990. Distribución de material mineral y azufre en los carbones de la formación Escucha. Relación con los factores geológicos, sedimentológicos y diagenéticos. Universidad de Barcelona, Barcelona.
Querol, X., Salas, R., Pardo, G., Ardevol, L., 1992. Albian coal-bearing deposits of the Iberian Range in northeastern Spain. Spain Geol. Soc. Am. 267, 193–208. https://doi.org/10.1130/SPE267-p193.
RFE, 2015. Real Farmacopea Española (RFE), fifth edition. Ministerio de Sanidad, Servicios Sociales e Igualdad, España.
Rodríguez-López, J.P., Meléndez, N., Soria, A.R., Boer, P.L., 2009. Reinterpretación estratigráfica y sedimentológica de las Formaciones Escucha y Utrillas de la Cordillera Ibérica. Rev. Soc. Geol. Esp. 22, 163–219.
Rodríguez-López, J.P., Meléndez, N., De Boer, P.L., Soria, A.R., 2010. The action of wind and water in a mid-cretaceous subtropical erg-margin system close to the Variscan Iberian Massif, Spain. Sedimentology 57, 1315–1356. https://doi.org/10.1111/j.1365-3091.2010.01147.x.
Rowe, R.C., Sheskey, P.J., Quinn, M.E., 2009. Handbook of Pharmaceutical Excipients, Sixth edition. Pharmaceutical Press, London.
Sánchez-Espejo, R., Aguzzi, C., Cerezo, P., Salcedo, I., López-Galindo, A., Viseras, C., 2014. Folk pharmaceutical formulations in western Mediterranean: Identification and safety of clays used in pelotherapy. J. Ethnopharmacol. 155, 810–814. https://doi.org/10.1016/j.jep.2014.06.031.
Sánchez-Espejo, R., Cerezo, P., Aguzzi, C., López-Galindo, A., Machado, J., Viseras, C., 2015. Physicochemical and in vitro cation release relevance of therapeutic muds "maturation". Appl. Clay Sci. 116–117, 1–7. https://doi.org/10.1016/j.clay.2015.08.007.
Sarruf, F.D., Contreras, V.J.P., Martinez, R.M., Velasco, M.V.R., Baby, A.R., 2024. The scenario of clays and clay minerals use in cosmetics/dermocosmetics. Cosmetics. https://doi.org/10.3390/cosmetics11010007.
Sayre, R.M., Agin, P.P., LeVee, G.J., Marlowe, E., 1979. A comparison of in vivo and in vitro testing of sunscreening formulas. Photochem. Photobiol. 29, 559–566. https://doi.org/10.1111/j.1751-1097.1979.tb07090.x.
Tang, W., Zhang, S., Gu, X., Sun, J., Jin, X., Li, H., 2016. Effects of kaolinite nanoroll on the flammability of polypropylene nanocomposites. Appl. Clay Sci. 132–133, 579–588. https://doi.org/10.1016/j.clay.2016.08.008.
Tang, W., Song, L., Liu, F., Dessie, W., Qin, Z., Zhang, S., Gu, X., 2022. Improving the flame retardancy and thermal stability of polypropylene composites via introducing glycine intercalated kaolinite compounds. Appl. Clay Sci. 217, 106411 https://doi.org/10.1016/j.clay.2022.106411.
Torres-Ruíz, J., López-Galindo, A., González-López, J.M., Delgado, A., 1994. Geochemistry of Spanish sepiolite-palygorskite deposits: Genetic considerations based on trace elements and isotopes. Chem. Geol. 112, 221–245. https://doi.org/10.1016/0009-2541(94)90026-4.
Vie, R., Azema, N., Quantin, J.C., Touraud, E., Fouletier, M., 2007. Study of suspension settling: a approach to determine suspension classification and particle interactions. Colloids Surf. A Physicochem. Eng. Asp. 298, 192–200. https://doi.org/10.1016/j.colsurfa.2006.10.074.
Viseras, C., Aguzzi, C., Cerezo, P., Lopez-Galindo, A., 2007. Uses of clay minerals in semisolid health care and therapeutic products. Appl. Clay Sci. 36, 37–50. https://doi.org/10.1016/j.clay.2006.07.006.
Vos, K., Vandenberghe, N., Elsen, J., 2014. Surface textural analysis of quartz grains by scanning electron microscopy (SEM): from sample preparation to environmental interpretation. Earth Sci. Rev. https://doi.org/10.1016/j.earscirev.2013.10.013.
Yuan, P., Tan, D., Annabi-Bergaya, F., Yan, W., Liu, D., Liu, Z., 2013. From platy kaolinite to aluminosilicate nanoroll via one-step delamination of kaolinite: effect of the temperature of intercalation. Appl. Clay Sci. 83–84, 68–76. https://doi.org/10.1016/j.clay.2013.08.027.
Zayd, H., Alsaeh, I.A., Mosa, F.A., Ben-Hander, G.M., 2019. In-Vitro Evaluation of Sun Protection Factors of Sunscreens Marketed in Sirte by Ultraviolet Spectrophotometry. J. Pure Appl. Sci. 18, 366–369.